Available online at www.sciencedirect.com
ScienceDirect
Journal of the European Ceramic Society 32 (2012) 283–289
www.elsevier.com/locate/jeurceramsoc

Solid particle impact erosion of alumina-based refractories at elevated temperatures

Jing-Zhou Yang [a,b], Ming-Hao Fang [a], Zhao-Hui Huang [a,*], Xiao-Zhi Hu [b], Yan-Gai Liu [a], Hao-Ran Sun [a], Jun-Tong Huang [a,c], Xiao-Chao Li [a]

[a] School of Materials Science and Technology, China University of Geosciences (Beijing), Beijing 100083, PR China
[b] School of Mechanical and Chemical Engineering, University of Western Australia, Perth, WA 6009, Australia
[c] Department of Engineering Materials, University of Sheffield, Sheffield S1 3JD, UK

Received 10 February 2011; received in revised form 28 July 2011; accepted 7 August 2011
Available online 9 September 2011

Abstract

Solid particle erosion tests have been conducted on three different alumina-based refractories at elevated temperatures up to 1400 °C, using sharp SiC particles between 325 and 830 μm in diameter. The impact speed is 50 m/s and the impact angle is varied between 30° and 90°. The objective of this study is to ascertain the effects of temperature and impact angle on the erosion resistance of alumina refractories. The experimental results reveal that the alumina-based refractories, in general, exhibit increasing erosion resistance with increasing temperature and decreasing impact angle, with the minimum erosion rate at 1200 °C and 30° impact angle. Chrome corundum refractory brick is the most resistant to vertical erosion, due to its highest alumina content, and associated hardness and density, as well as strongly bonded aggregate and binder phase. The primary material removal mechanisms are fracture and chipping of binder phase and aggregate, as well as aggregate pull-out.

Keywords: Al_2O_3; Refractories; Wear resistance; Composites; Surface

1. Introduction

High-temperature solid-particle erosion wear, which can cause major damage and failure of many industrial equipments and facilities, is a serious issue in coal-fired thermal power stations, cement industry, garbage incineration, petrochemical industry, and metallurgical industry. For instance, refractory materials used in a slagging gasifier, are subject to "erosion wear" due to the combination of chemical and mechanical interaction with the refractories. The causes of such erosion wear may include chemical corrosion of molten slag/hot gas/molten salt and physical wears of high velocity particulate/flowing slag erosion, creep, thermal shock damage and spalling.[1] To avoid misunderstanding, it is essential to clarify in this paper that the "erosion wear" only refers to the physical action of "solid particle erosion".

Erosion wear or "solid particle erosion" at elevated temperatures is an even more special, yet important, issue. The refractory lining materials for circulating fluidized bed (CFB) furnace are commonly eroded between 850 °C and 1100 °C by the coal powders, high-melting mineral impurity particles and limestone grits for desulfurizing. The refractory linings of dry-process cement kiln, cyclone separator and garbage incinerator are also subject to similar erosion wear at various elevated temperatures by clinker, dust and garbage. Their services can be severely shortened by such high temperature erosion wear. Therefore it is essential to fully understand the process and mechanisms of the high temperature erosion of commonly used refractories, which in turn will help to develop new generation of refractories with improved erosion wear performance.

It is noted that a number of studies have been done on the solid particle erosion at elevated temperature for metals and ceramic materials.[2–8] Key erosion mechanisms have been studied using micro-cutting model and elastic–plastic fracture mechanics.[9–16] Yet, little work on the erosion wear of refractories has been reported in the literature. Refractories consisting of very coarse and fine aggregates and binder phase, is very different to

* Corresponding author. Tel.: +86 10 82322186; fax: +86 10 82322186.
E-mail address: huang118@cugb.edu.cn (Z.-H. Huang).

0955-2219/$ – see front matter © 2011 Elsevier Ltd. All rights reserved.
doi:10.1016/j.jeurceramsoc.2011.08.017

Table 1
Chemical compositions and properties of three alumina based refractory bricks.

Property	Brick type		
	HAB	CMB	CCB
Chem. (wt.%)*			
$-Al_2O_3$, ≥	70	75	87
$-Cr_2O_3$, ≥	NL	NL	12
$-SiO_2$, ≤	NL	NL	0.3
$-Fe_2O_3$, ≤	1.5	0.8	0.4
Cold compression strength (MPa)*, ≥	60	120	120
Bending strength (MPa)	15.9–17.8**	16–23[a]	16.2–31.7[b]
Vickers hardness of aggregates (GPa)**	11.2	12.5	13.7
Vickers hardness of binder phase (GPa)**	9.8	10.2	11.8
Apparent porosity (%)*, ≤	21	18	17
Bulk density (g/cm^3)*, ≥	2.8	2.9	3.3
Apparent porosity (%)**	22	12.7	14.5
Bulk density (g/cm^3)**	2.7	2.9	3.1

* Data from manufacturer's technical publication. NL, not listed.
** Data from laboratory measurements.
[a] Cai[19].
[b] Li[20].

fine-grained and more uniform ceramics and metals. Therefore, the primary objective of this paper is to compare the high temperature erosion wear performances of three commonly used alumina based refractories, i.e. high alumina brick, corundum-mullite brick and chrome corundum brick. It is also attempted to ascertain the effects environmental temperature and impact angle on the erosion resistance of alumina refractories. Digital camera, optical and scanning electron microscopes are used to characterize the erosion characteristics and identify the major erosion mechanisms.

2. Materials and methods

Solid particle erosion tests were carried out on the commercial alumina-based refractories of high alumina brick (HAB), corundum-mullite brick (CMB) and chrome corundum brick (CCB) sourced from Luoyang refractory Co., China. Their chemical compositions and fundamental properties are listed in Table 1. The target for vertical/normal erosion had a dimension of 12 cm × 12 cm × 3 cm. Standard refractory bricks were cut into different angular blocks, as the targets for oblique erosion. The erosion tests were performed using an in-house designed high-temperature (up to 1400 °C) solid particle erosion equipment in accordance with ASTM G76-04. Its schematic diagram is shown in Fig. 1. As can be seen, the nozzle, target and erosion chamber are in the furnace. The recrystallized silicon carbide erosion chamber is for protecting the heating unit and furnace lining from erosion damage. Angular black silicon carbide grits (97% of particles are within the size range of 325–830 μm) were used as impact/erodent particles. The impact particles are accelerated in an air stream down a glass tube (diameter 10 mm) and corundum ceramic nozzle (diameter 20 mm) to impact on the targets at 25 °C, 1000 °C, 1200 °C and 1400 °C. The stand-off distance, from the end of the nozzle to the surface of the target, was 10 cm. The feeding rate of impact particles was 60 g min^{-1}. The duration of each test was 5 min, during which about 300 g of SiC particles had impacted the target surface. The impingement angles of gas-particle stream on the targets were 30°, 45°, 60°, 75° and 90°. The impact velocity was 50 m/s measured by the rotating double-discs method.[17] For high temperature erosion, it is essential to pre-heat the targets to minimize the effect of thermal shock on the erosion damage. The solid particle erosion resistance was characterized with the volume erosion rate, which was defined as the volume loss of specimen material divided by the total mass of abrasive particles (mm^3 g^{-1}) as shown by Eq. (1).[18]

$$\text{volume erosion rate} = \frac{\text{average mass loss}}{\text{test time}} \times \frac{1}{\text{particle flux}} \times \frac{1}{\text{specimen density}} \quad (1)$$

Bulk density and apparent porosity were measured using the Archimedes water immersion method. The alumina refractory bricks were cut into bars of 100 mm × 20 mm × 20 mm. The bending strength was determined using a conventional

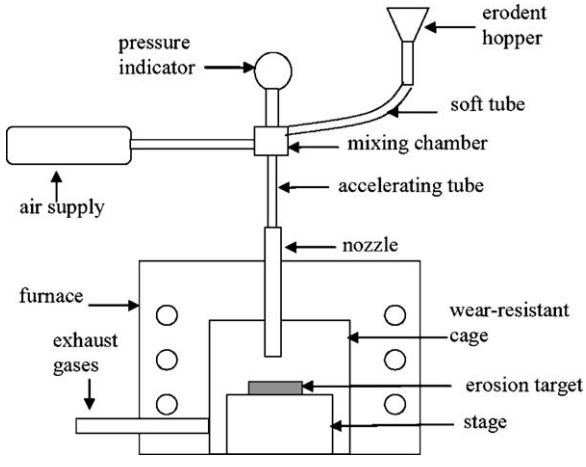

Fig. 1. Schematic of the high-temperature solid particle erosion apparatus.

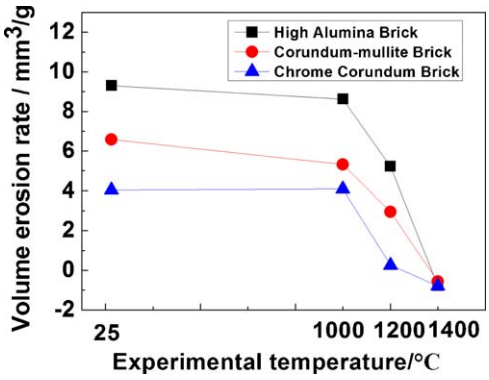

Fig. 2. The volume erosion rates of alumina-based refractories with respect to the test temperature.

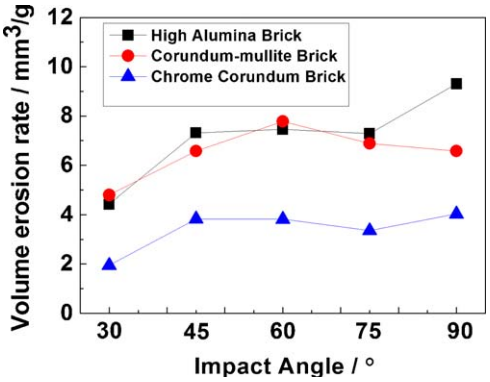

Fig. 3. The volume erosion rates of the alumina-based refractories with respect to the impingement angle at room temperature.

three-point bending method with a support roller span of 80 mm at a crosshead speed of 0.5 mm/min. The Vickers hardness was examined under a load of 0.2 kg, held for 15 s. The compositions and physical properties are listed in Table 1.

Optical microscopy and scanning electron microscopy (SEM) (JSM 6460LV) were used to characterize the original and erosion surfaces

3. Results and discussion

In order to compare the high temperature erosion wear performances of the three alumina-based refractories, it is essential to clearly understand their similarities and differences. Although Al_2O_3 is the main component for all three refractory bricks, the percentage content is different. As shown in Table 1, it is about 87.0 wt.% for chrome corundum brick (CCB), 80.0 wt.% for corundum-mullite brick (CMB), and only 70.0 wt.% for high alumina brick (HAB). It should be mentioned that traditional refractories commonly consist of aggregates and binder phases/matrixes. Aggregates are normally refractory particles with the diameters over 0.044 mm. It is also reported that 1–3 mm and −1 mm aggregates are usually used for shaped alumina based refractories.[21,22] For HAB, calcined bauxite or chamotte particles are usually used as the raw aggregates, and industrial alumina or refractory clay powders as raw binders. After sintering, the main phases in HAB contain mullite, corundum and glassy phase.[23,24] White fused corundum and mullite particles are mainly raw aggregates for CMB. Industrial alumina and silica or mullite or refractory clay micro powders are used as raw binders.[25] Main phases of aggregates for sintered CMB are corundum and mullite. Most of the binder phase is micro-crystalline mullite. With the addition of about 10 wt.% Cr_2O_3, CCB is a special kind of refractory with significant compositional and micro-structural differences to HAB and CMB. The main phases are solid solution Cr_2O_3–Al_2O_3.[26,27] Pink fused corundum particles and Cr_2O_3–Al_2O_3 powders are respectively used as raw aggregates and binders. In the sintered CCB, the aggregates and binder are tightly bonded by the micro-crystalline Cr_2O_3–Al_2O_3, which improves its strength and resistance to mechanical damage. On the basis of data in Table 1 and the above discussion, what we could expect is that CCB should show better erosion resistance compared with CMB and HAB. And HAB would be the least resistant to solid particle erosion damage at room temperature.

Fig. 2 shows the volume erosion rate of HAB, CMB and CCB as a function of the test temperature. As can be seen, the erosion rate tends to slightly decrease with increasing the test temperature from 25 °C to 1000 °C, then sharply decline from 1000 °C to 1400 °C. The possible reasons are as follows. At high temperatures, the aggregates would expand to some extent and create residual compressive stresses within the binder phase, which could improve the overall strength and erosion resistance of the refractory brick. Also at elevated temperatures, the binder phase is softer and can accommodate more plastic deformation. So more impact energy can be consumed and absorbed. The alumina-based refractories show improved erosion performance with elevating the test temperature. At 1200 °C, they exhibit the best erosion resistance. As might be expected, the erosion resistance of CMB is between those of CCB and HAB. CCB is the most resistant to erosion damage. The reason may relate to their various mechanical properties, phase compositions, and porosities. CMB and CCB have better strengths and lower porosities than that of HAB, as shown in Table 1. CCB has more corundum phase than that of CMB. And the main phase in HAB is mullite. As listed in Table 1, the Vickers hardness of aggregate in HAB, CCB and CMB is respectively 11.2 GPa, 12.5 GPa and 13.7 GPa. The hardness of their binder phase is sequentially

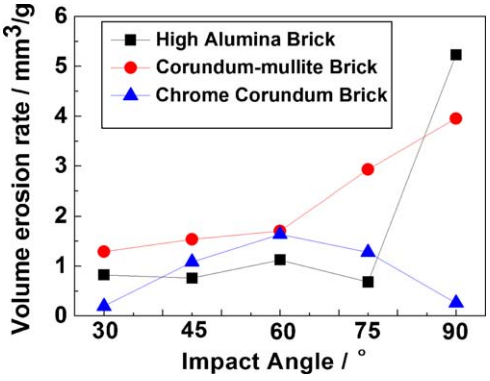

Fig. 4. The volume erosion rates of the alumina-based refractories with respect to the impingement angle at 1200 °C.

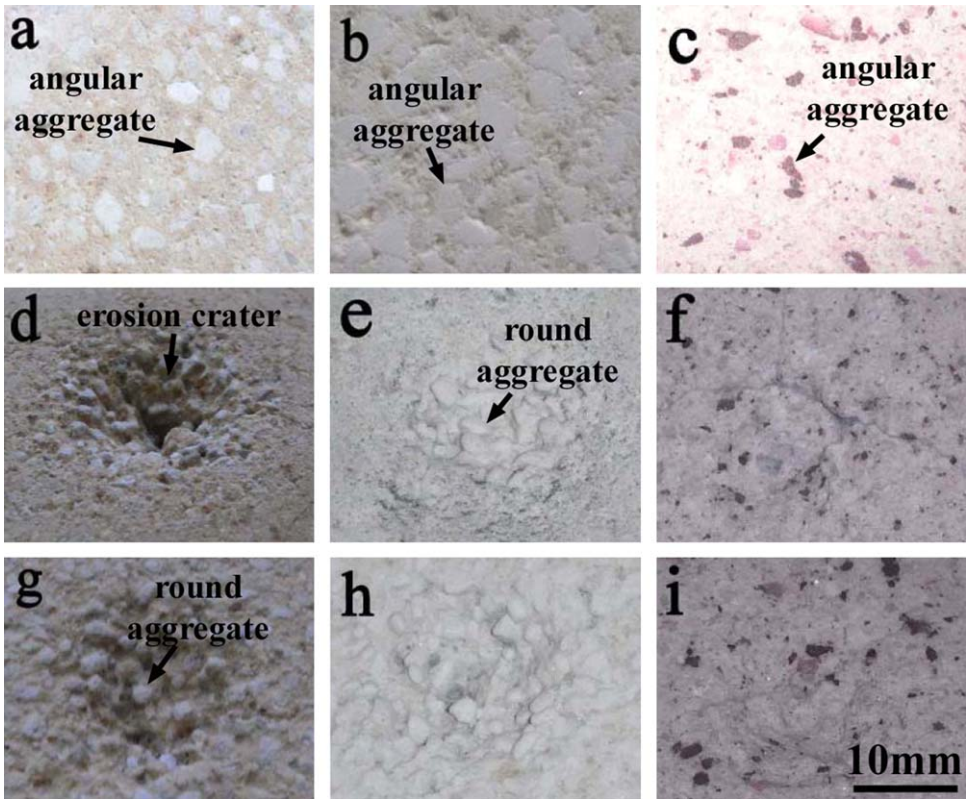

Fig. 5. The photographs showing the original and eroded surfaces of the alumina based refractories at the impingement angle of 90°: the original surfaces of (a) high alumina brick (HAB), (b) corundum-mullite brick (CMB) and (c) chrome corundum brick (CCB); the eroded surfaces of (d) HAB, (e) CMB and (f) CCB at room temperature; the eroded surfaces of (g) HAB, (h) CMB and (i) CCB at 1200 °C.

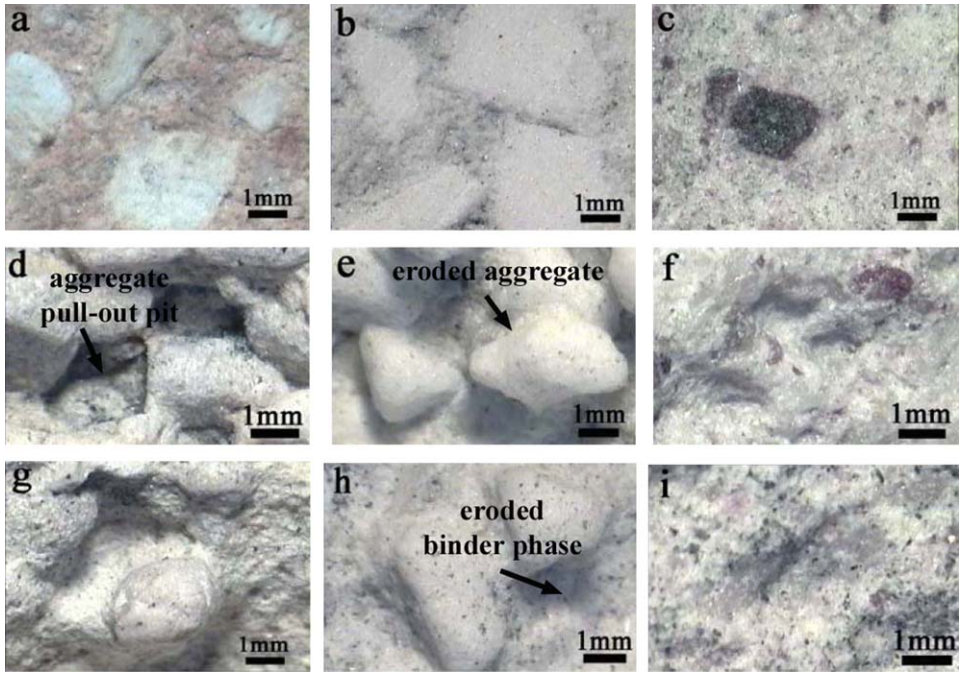

Fig. 6. The optical micrographs showing the original surfaces and erosion morphologies of the targets at the impingement angle of 75°: the original surface of (a) high alumina brick (HAB), (b) corundum-mullite brick (CMB) and (c) chrome corundum brick (CCB); the erosion morphologies of (d) HAB, (e) CMB and (f) at room temperature; the erosion morphologies of (g) HAB, (h) CMB and (i) CCB at 1200 °C.

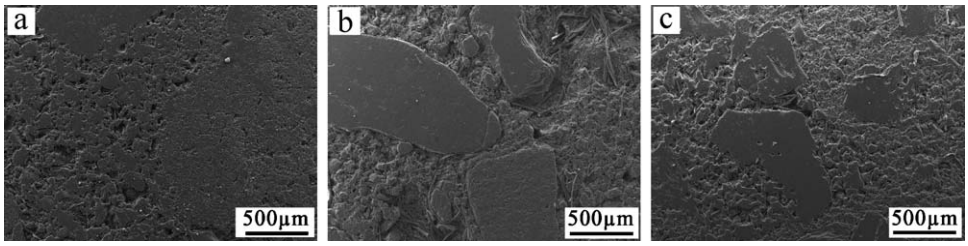

Fig. 7. SEM images showing microstructures of (a) high alumina brick; (b) corundum-mullite brick and (c) chrome corundum brick.

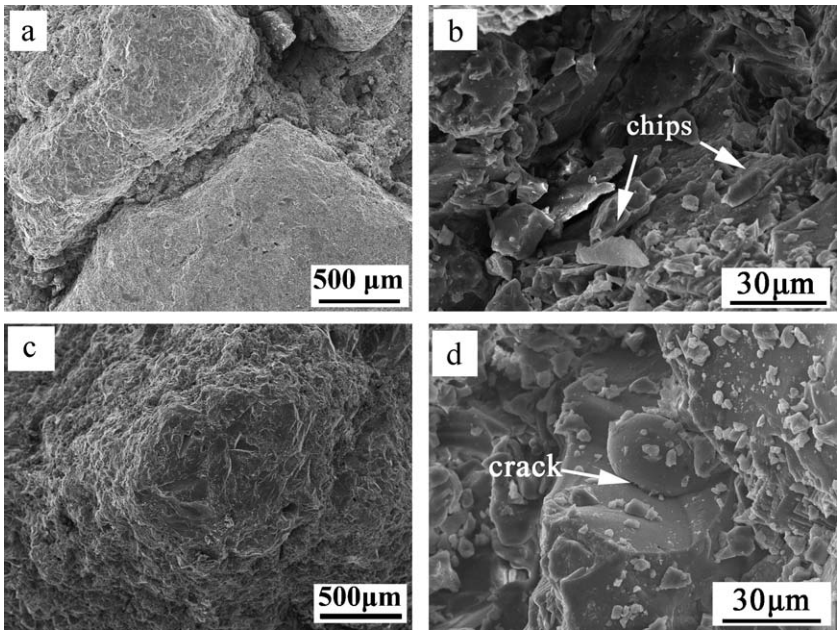

Fig. 8. Erosion morphologies of alumina-based refractories for vertical erosion at room temperature: (a) overview and (b) enlarged photo for corundum-mullite brick; (c) overview and (d) enlarged photo for chrome corundum brick.

9.8 GPa, 10.2 GPa and 11.8 GPa. It is obvious that CCB has the highest hardness for binder phase and aggregate. Besides, the bending/compression strength of CCB is higher than those of HAB and CMB as shown in Table 1. So CCB exhibits better erosion resistance compared with HAB and CMB.

Note that the erosion rate at 1400 °C is negative. Because, in this case, SiC impact particles adhered on all the eroded samples due to the self-contained and melt glass contaminant from the accelerating tube, leading to a mass gain and invalid negative erosion rate of the impacted samples. Therefore only the erosion properties at 25 °C, 1000 °C, and 1200 °C were discussed above.

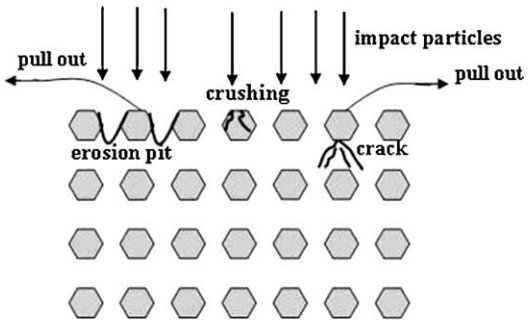

Fig. 9. Schematic diagram of material removal process for refractories impacted by hard particles.

Fig. 3 shows the volume erosion rate as a function of the impingement angle at room temperature. The erosion rate is found to be strongly dependent on the impingement angle, increasing notably with increasing the impingement angle. For HAB and CCB, it reaches the highest value at 90°, twice of that at 30°. For CMB, maximum erosion rate occurs at 60°. As is well known, for typical brittle materials, maximum impact erosion rate usually occurs at 90°. It is always for impact at 15–30° for typical ductile materials. At room temperature, refractories are brittle materials. And for normal erosion, the impact energy of erodent particles acting on the target surface is much more than that for oblique erosion. It should be mentioned that the erosion rate data shows CCB is more resistant to impact damage for the erosion at room temperature compared with HAB and CMB.

Fig. 4 shows the volume erosion rate as a function of impingement angle at 1200 °C. The erosion rate increases notably with increasing the impingement angle. For HAB and CMB, it reaches the highest value for erosion at 90°. For CCB, maximum erosion rate appears for erosion at 60°. It can be concluded that the alumina-based refractories exhibit better erosion perfor-

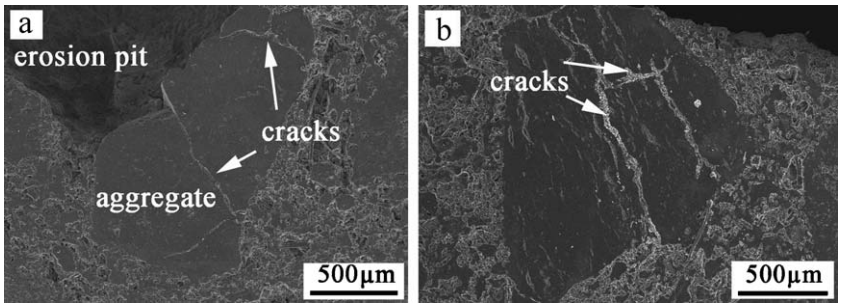

Fig. 10. Cross-sectional view showing the cracks in aggregate located at the bottom of erosion pit.

mance at low impingement angles than that at high angles. Note that the erosion rate data shows HAB is more resistant to impact damage for oblique erosion at 1200 °C compared with CMB and CCB, just opposite to that for the normal erosion.

Fig. 5 displays photos showing the original and eroded surfaces of the alumina-based refractories for the erosion at 90°. It can be seen that after the erosion tests were conducted, the angular aggregates became rounder and more exposed due to impact and micro-cutting of the SiC erodents. The binder phase was heavily eroded. The damage craters for the erosion at room temperature are deeper than those at 1200 °C, which shows that the targets have better erosion resistances at 1200 °C. As shown in Figs. 5(d)–(f), the erosion craters for the three kinds of alumina-based refractories have nearly the same diameter of about 30 mm, but different depths of 10 mm for HAB, 5 mm for CMB and 3 mm for CCB. And more exposed aggregates can be found in the eroded surfaces of HAB and CMB compared with CCB, which indicates that CCB has a stronger binder phase and aggregates/binder bonding interface, and eventually the better erosion resistance.

Fig. 6 shows the optical micro-morphologies of the original and eroded surfaces of the alumina-based refractories for the erosions at 75°. From Fig. 6(a)–(c), the angular aggregates with diameters of 2–5 mm can be found in the raw refractory targets, which is similar to what has been shown in Fig. 5(a)–(c). They become rounder after the erosion at room temperature and 1200 °C as shown in Fig. 6(d)–(i). The binder phases were eroded heavily because of the higher porosity compared with the aggregates. As can be seen from Fig. 6(d), (e), (g) and (h), the aggregates were exposed after the binder phases were removed from HAB and CMB. And the aggregates pull-outs occurred in the erosion process as shown in Fig. 6(d). The material removal resulted from the fracturing and chipping of the binder phase and aggregates, as well as the aggregates pull-outs, which is very similar to the erosion mechanism[28,29] for cermets, for example, WC-Co/Cr, Because refractories and cermets are both composed of hard aggregates/particles and soft binder phases.

The binder phase of CCB exhibits higher hardness and better erosion resistance compared with HAB and CMB, which is supported by the values listed in Table 1 and the shallower erosion craters shown in Fig. 6(f) and (i). Few exposed aggregates can be found in the eroded surface of CMB, due to the protection of binder phase. So it is essential for the refractories to have a hard and strong binder phase for achieving good erosion resistance.

In order to understand the microstructure of the three alumina based refractories, SEM observation was carried out on their polished surfaces. The typical images are shown in Fig. 7. As can be seen, the most of aggregates are angular and more than 0.5 mm in diameter. The binder phase is quite porous, which is not beneficial to the erosion wear resistance of the refractories. Both the aggregate and binder phase of HAB have much higher porosity compared with CMB and CCB, which supports that HAB shows poorer erosion resistance.

Fig. 8 shows the overview and enlarged photo of eroded aggregates and binder phases in CMB and CCB. As can be seen, the corundum and chrome corundum aggregates have rounder surfaces compared with the un-eroded angular ones. It should be mentioned that the softer binder phases are eroded more heavily compared with the aggregates as shown in Fig. 8(a) and (c), which is similar to what has been shown in Fig. 6. Enlarged SEM photos of eroded surface are shown in Fig. 8(b) and (d). Some small chips and micro-cracks can be found. The binder phase and aggregate in the top surface cracks and fractures due to the impact of the erodent particles. Then the material is removed as chips. It is proposed that brittle erosion mechanism is dominant for the material removal of refractories eroded at room temperature.

Refractories consisting of coarse aggregate and binder phase are brittle materials. So the brittle erosion mechanism should dominate the material removal. As reported by Evans et al.[12] and Lawn et al.[30], radial and lateral cracks occur when the brittle materials are eroded by hard particles. The former decreases the strength of the target, yet the latter leads to the material removal. In a similar way, cracks generate and propagate in the binder phase and aggregate for refractories impacted by erodent particles. After that, big erosion pits occur in the binder phase and some aggregates are dislodged, as shown in Fig. 9. It should be mentioned that cracks could also occur in the subsurface due to the accumulated impact stress and energy of the erodent particles, which has a significant contribution to the dislocation of millimetre-sized aggregates. Fig. 9 displays the material removal process for the refractories, which was further confirmed by the cross-sectional observation of the damaged area. SEM images in Fig. 10 show that cracking has occurred in the aggregates, indicating brittle erosion does occur in those refractories.

4. Conclusions

This study has compared the erosion wear resistances of three commercial alumina-based refractories, high alumina brick (HAB), corundum-mullite and chrome corundum bricks (CMB and CCB), which were measured at a range of temperatures from room temperature to 1400 °C, and with the solid-particle impact angles from 30° to 90°. Based on the experimental results and associated discussions in the previous section, the following conclusions can be drawn.

(1) All three alumina-based refractories show increasing erosive wear resistance with increasing temperature, and decreasing impact angle. However, the minimum erosion took place at 1200 °C and with the impact angle of 30°, the lowest impact angle tested.
(2) CCB has better erosion resistance than those of HAB and CMB, consistent with their alumina percentage and mechanical properties.
(3) The material removal is mainly resulted from fracture and chipping of the binder phase and aggregates, as well as the aggregates pull-outs. Those brittle erosion mechanisms still dominate the material removal of those refractories due to solid particle impact erosion at elevated temperatures.
(4) To optimize the erosion resistance, alumina-based refractories should have hard aggregates and strong binder phases, in addition to low porosity.

Acknowledgements

The authors greatly appreciate National Natural Science Foundation of China for financial support (Grant Nos. 50572098, 50802091, and 50972134). We also thank the Fundamental Research Funds for the Central Universities (Grant No. 2009PY09, 2009PY10 and 2010ZD12). J.-Z. Yang is supported by China Scholarship Council. Z.-H. Huang is supported by Gledden Visiting Senior Fellowship from University of Western Australia in 2010.

References

1. Bennett JP, Kwong K-S. *Refractory liner materials used in slagging gasifiers*. *Refract Appl News* 2004;**9**(5):20–5.
2. Goretta KC, Cunninghama AJ, Chen N, Singh D, Routbort JL, Rateick Jr RG. *Solid-particle erosion of an anodized Mg alloy*. *Wear* 2007;**262**:1056–60.
3. Hussainova I, Pirso J, Antonov M, Juhani K. *High temperature erosion of Ti(Mo)C–Ni cermets*. *Wear* 2009;**267**:1894–9.
4. Alman DE, Tylczak JH, Hawk JA, Schneibel JH. *An assessment of the erosion resistance of iron–aluminide cermets at room and elevated temperatures*. *Mater Sci Eng A* 2002;**329–331**:602–9.
5. Kim JJ. *Solid particle erosion of hot-pressed silicon nitride*. *J Mater Sci* 2006;**41**:6178–80.
6. Ham AL, Yeomans JA, Watts JF. *Effect of temperature and particle velocity on the erosion of a silicon carbide continuous fibre reinforced calcium aluminosilicate glass–ceramic matrix composite*. *Wear* 1999;**233–235**:237–45.
7. Alman DE, Tylczak JH, Hawk JA, Hebsur MG. *Solid particle erosion behavior of a Si_3N_4–$MoSi_2$ composite at room and elevated temperatures*. *Mater Sci Eng A* 1999;**261**:245–51.
8. Zhou JR, Bahadur S. *Erosion characteristics of alumina ceramics at high temperatures*. *Wear* 1995;**181–183**:178–88.
9. Walley SM, Field JE. *The contribution of the Cavendish Laboratory to the understanding of solid particle erosion mechanisms*. *Wear* 2005;**258**:552–66.
10. Zhou JR, Bahadur S. *The effect of material composition and operational variables on the erosion of alumina ceramics*. *Wear* 1991;**150**:343–54.
11. Wiederhorn SM, Hockey BJ. *Effect of material parameters on the erosion resistance of brittle materials*. *J Mater Sci* 1983;**18**:766–80.
12. Evans AG, Gulden ME, Rosenblatt ME. *Impact damage in brittle materials, in the elastic–plastic response regime*. *Proc R Soc Lond, Ser A* 1979;**361**:343.
13. Finnie I. The mechanism of erosion of ductile metals. In: Haythornthwaite RM, editor. *Proceedings of the third US national 179 congress on applied mechanics*. New York: Am Soc Mech Eng; 1958. p. 527–32.
14. Bitter JGA. *A study of erosion phenomena: part I*. *Wear* 1963;**6**:5–21.
15. Hutchings IM. *A model for the erosion of metals by spherical particles at normal incidence*. *Wear* 1981;**70**:269–81.
16. Sheldon GL, Finnie I. *On the ductile behaviour of nominally brittle materials during erosive cutting*. *Trans ASME, J Eng Ind* 1966:8348–99.
17. Ruff AW, Ives LK. *Measurement of solid particle velocity in erosive wear*. *Wear* 1975;**35**:195–9.
18. ASTM G76-04. Standard test method for conducting erosion tests by solid particle impingement using gas Jets.
19. Cai Y-Z, Yang B, Wang G. *Effect of silica sol on mechanical properties of mullite bonded corundum refractory*. *J Chin Cream Soc* 2007;**35**:664–70 (in Chinese).
20. Li D, Chen R. *Application of corundum brick and chrome–corundum brick*. *Refractories* 2001;**35**:31–3 (in Chinese).
21. Aksel C. *The influence of zircon on the mechanical properties and thermal shock behaviour of slip-cast alumina-mullite refractories*. *Mater Lett* 2002;**57**:992–7.
22. Amrane B, Ouedraogo E, Mamen B, Djaknoun S, Mesrati N. Experimental study of the thermo-mechanical behaviour of alumina-silicate refractory materials based on a mixture of Algerian kaolinitic clays. doi:10.1016/j.ceramint.2011.05.095.
23. Abou-Sekkina MM, Abo-El-Enein SA, Khalil NM, Shalma OA. *Phase composition of bauxite-based refractory castables*. *Ceram Int* 2011;**37**:411–8.
24. McGee TD, Dodd CM. *Mechanism of secondary expansion of high-alumina refractories containing calcined bauxite*. *J Am Ceram Soc* 1961;**44**:277–83.
25. Aksel C. *The effect of mullite on the mechanical properties and thermal shock behaviour of alumina-mullite refractory materials*. *Ceram Int* 2003;**29**:183–8.
26. Davies TJ, Emblem HG, Nwobodo CS, Ogwu AA, Tsantzalou V. *Preparation and properties of some alumina-chrome refractories*. *J Mater Sci* 1991;**26**:1061–8.
27. Al-Douri WA, Davies TJ, Ogwu AA, Emblem HG. *Solid state chemistry of alumina–chromia–magnesia and related refractories*. *J Mater Sci* 1994;**13**:1543–5.
28. Gee MG, Gee RH, McNaught I. *Stepwise erosion as a method for determining the mechanisms of wear in gas borne particulate erosion*. *Wear* 2003;**255**:44–54.
29. Barber J, Mellor BG, Wood RJK. *The development of sub-surface damage during high energy solid particle erosion of a thermally sprayed WC-Co–Cr coating*. *Wear* 2005;**259**:125–34.
30. Lawn BR, Swin MV. *Microfracture beneath point indentations in brittle solid*. *J Mater Sci* 1975;**10**:113–22.